Event and object selection for the measurement of vector boson scattering in WZ+2jets events with ATLAS Run-3 data - A Summer Student Report

Risako Tagami (The University of Tokyo)

Supervisors : Angela Maria Burger, Valentina Cairo

Abstract

Vector Boson Scattering (VBS) is an important test of the Standard Model and the electroweak symmetry breaking mechanism. Our final goal is to measure the boson polarization in WZ+2jets events with ATLAS Run-3 data. First of all, there are needs to check the modeling of the current simulation and to optimize object selection in order to maximize the sensitivity of the analysis.

I report the modeling of the current simulation and optimization studies.

1. Introduction

Since the Higgs boson was discovered for the first time in 2012 using data from the ATLAS[1][2] and CMS[3] experiments at the Large Hadron Collider (LHC), the studies related to Higgs and beyond the standard model have been actively pursued.

Vector Boson Scattering (VBS) has become a very exciting test to probe the electroweak symmetry breaking mechanism. VBS was observed for the first time with CMS using 35.9fb^{-1} during 2015+2016 in electroweak production of two W bosons with the same charge associated with 2 jets[4]. VBS of WZ was observed for the first time in association with 2 jets with ATLAS using 36fb^{-1} of data taken during Run-2 of the LHC during 2015+2016 with a center mass energy of 13 TeV[5] and in CMS with full Run-2 data (137fb^{-1}, 2016-2018)[6].

When longitudinally polarized gauge bosons scatter, the cross-section grows indefinitely with energy and violates the unitarity principle. The longitudinal polarization modes of the massive vector bosons are strongly tied to the electroweak symmetry breaking mechanism. The unitarity is usually preserved by the Higgs boson, hence we can validate the predictions of the Standard Model. Measurements of gauge boson polarization through VBS have been done during Run-2 of the LHC for example by the ATLAS Collaboration[7][8]. The final goal is to measure the boson polarization with the data of Run-3 of the LHC in ATLAS.

Our signal and the dominant background are as Figure 1. Our signal is EW produced WZ diboson events in association with two hadronic jets ("WZjj-EW", $\mathcal{O}(\alpha_{\rm EW}) = 6, \mathcal{O}(\alpha_{\rm S}) = 0$). Typically, the trajectories of the incoming quarks are altered only slightly when the gauge bosons are radiated, and then the two jets are seen in the forward regions close to the beam direction. The W boson decays into a pair of lepton and neutrino which manifests as missing momentum in the transverse direction, and Z boson decays into a pair of leptons with same flavor but opposite charge. The dominant background is QCD production ("WZjj-QCD", $\mathcal{O}(\alpha_{\rm EW}) = 4$).

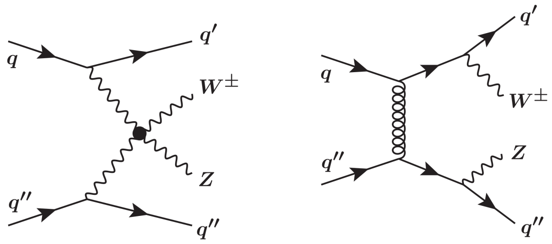

Figure 1: Feynman diagrams of the signal process WZjj-EW (left) and of the most dominant background WZjj-QCD (right).

The WZjj-EW simulation which will be used to model the signal in Run-3 is validated against the simulation for Run-2. Further, the object selection is optimized to increase the sensitivity of the analysis.

The data used in this study are Run-2 (2015-2018) and Run-3 (2022) ATLAS data.

2. Selection

We define a region enriched in signal events, denoted signal region. We followed the selection as in the previous WZ+2jets vector boson scattering measurements with full Run-2 ATLAS data during 2015-2018[9]. Our signal region selection is as Table 1.

Table 1: Signal region selection. p_T: transverse momentum, η: $-\ln\left(\tan\frac{\theta}{2}\right)$, SFOC: same flavor, opposite charge

$\mathrm{N_{lep}} == 3$ (e/μ)
At least one lepton pair w/ SFOC, $\lvert m(l_1, l_2) - m_Z \rvert < 10$GeV –> Z-boson
$m_{\mathrm{T}}^{\mathrm{W}} > 30\mathrm{GeV}^1$
Njets>= 2
$p_{\mathrm{T,jet}}^{\mathrm{lead}} > 40$ GeV ("jet1")
remaining jet with largest p_{T} with $\eta_{\mathrm{jet1}} \cdot \eta_{\mathrm{jet2}} < 0$
$m(\mathrm{jet1}, \mathrm{jet2}) > 500\mathrm{GeV}$
$N_{\mathrm{jet,b-tag}} == 0$

[1] $m_{\mathrm{T}}^{\mathrm{W}} = \sqrt{2p_{\mathrm{T}}^{\nu} p_{\mathrm{T}}^{l}\left[1 - \cos\Delta\phi(l, \nu)\right]}$

Z-boson is reconstructed using the first and the second lepton (l_1, l_2), while W-boson is reconstructed using the third lepton (l_3).

The definition of fiducial phase space in this study follows closely the one defined in the previous study[9]. Fiducial phase space is defined at truth level using truth particles and to be close to the measurement phase space which is given by the detector acceptance and the selection cuts. Reconstructed level (reconstructed phase space) is defined as reconstructed particles after the detector simulation, simulating reconstruction/selection efficiencies. To know the accurate cross section, the efficiency of the detector should be known.

3. Signal Region Selection

The expected number of events in the signal regions listed by process can be seen in Table 2.

Name	Number of events
WZjj-EW (signal)	26.41
WZjj-QCD	125.91
Zgamma	7.80
ttbarV	8.02
ZZ	49.50
VVV	0.61
tZ	4.09

Table 2: Number of events of signal or each background.

Z+jets and ttbar simulations are not available yet, however their expected signal region contribution is about 5 %. Current simulated events in the signal region is as Figure 2.

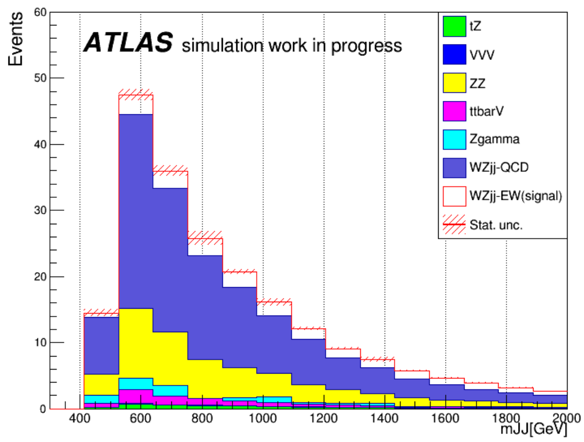

Figure 2: Simulated events of the invariant mass of the two selected tagging jets in the signal region. The events have at least two jets, and the highest two jets are tagged and defined as "two selected tagging jets". This is scaled to 2022 luminosity.

WZjj-QCD is by far the most important background.

4. Searching for discriminating variables

WZjj-EW is a rare process and difficult to distinguish from the dominant background (WZjj-QCD) because their final state are completely the same and they are different only kinematically. It is important to find variables which discriminate best the signal from the background for reducing correlation and impact of the background systematics.

To evaluate the discriminating power, I made plots of WZjj-EW and WZjj-QCD, calculated mean value, standard deviation and separation score $\langle S^2 \rangle$ [10], fitted the plots to general distribution. The definition of separation score:

$$\langle S^2 \rangle = \frac{1}{2} \int \frac{(\hat{y}_{\mathrm{S}}(y) - \hat{y}_{\mathrm{B}}(y))^2}{\hat{y}_{\mathrm{S}}(y) + \hat{y}_{\mathrm{B}}(y)} dy. \quad (\hat{y}_{\mathrm{S}} : \text{signal distribution}, \ \hat{y}_{\mathrm{B}} : \text{background distribution}) \tag{1}$$

One of the examples of comparison is as Figure 3.

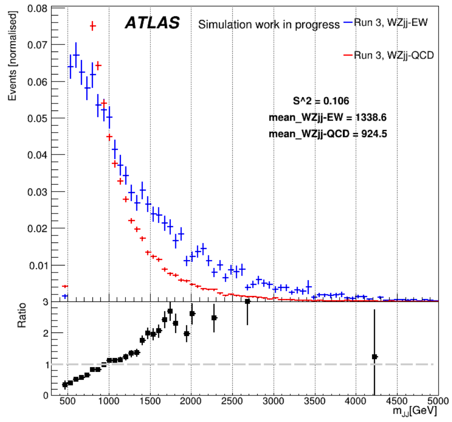

Figure 3: Comparison of WZjj-EW and WZjj-QCD using invariant mass of the two selected tagging jets.

Other examples are in the back up section. Some variables are tested, and currently, m_{JJ} (the invariant mass of the two selected tagging jets), $Deta_{JJ}$ ($\Delta\eta$ of the two selected tagging jets), RpThard (transverse component of the vector sum of W,Z and tagging jets momenta divided by their scalar pT sum) and centrality[9] (centrality of the WZ system,) have decent discriminating power according to the separation score and the plots.

In the future, deep neural network could be utilized by using those variables to discriminate signal better. Another way to reduce the impact of backgrounds systematics is to reduce the contamination of the signal region by background processes. This will be discussed in section 7.

5. Background modeling

Confidence in the background modeling allows us to reduce uncertainties on the background.

5.1 Control regions

We defined control regions enriched with dominant background processes to check the modelings of the backgrounds. The control regions we defined are kinematically close to the signal region in order to be extrapolated the findings in the control regions easily to the signal region.

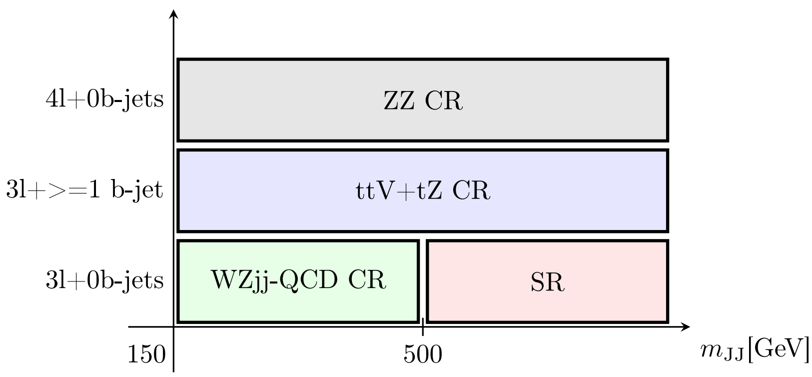

Figure 4: Control regions

5.2 Agreement of data and simulated data in each control regions

Current agreement between data and simulated data of each control regions are as below.

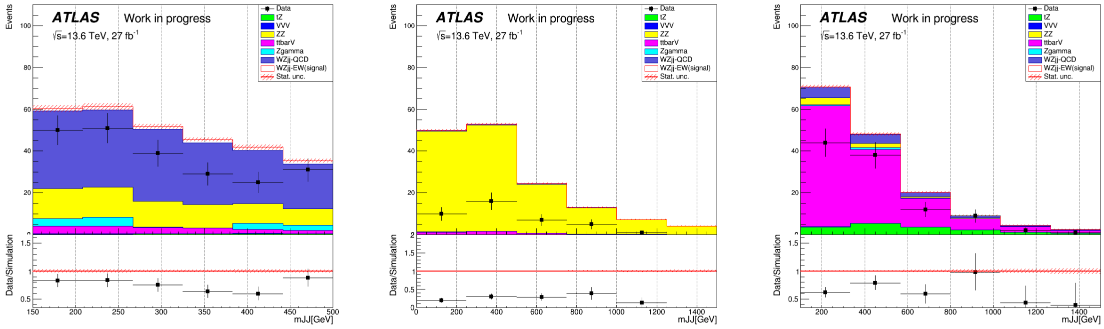

Figure 5: ATLAS Run-3 2022 data with simulated data of QCD-CR(left), ZZ-CR(center), ttV+tZ-CR(right). Z+jets and ttbar are still missing, but their expected contribution is 5%.

In the ZZ-CR plot in Figure 5, there is unexpected disagreement between the data and simulated data. It seems that ZZ-CR has normalization problem. In the end, this problem need to be corrected. In the QCD-CR plot and the ttV+tZ-CR plot in Figure 5, the data undershoot the simulations, but corrections are expected to be around 20 %.

6. Comparison between Run-2 and Run-3 simulated events

Run-2 and Run-3 WZjj-EW and WZjj-QCD simulations are compared. Run-2 and Run-3 simulations are different in terms of pp center-of-mass energy, Sherpa[11] version and the software release:

- Run-2 : center of mass energy = 13 TeV, Sherpa 2.2.12 (Rel. 21)
- Run-3 : center of mass energy = 13.6 TeV, Sherpa 2.2.14 (Rel. 22)

Although there are differences regarding the above point, they are expected not to have a big impact to events, hence their kinematic distributions are expected to be similar. It's important to compare different versions of simulated events to validate simulation data and also to know the effect of the differences.

6.1 Comparison of selection efficiency

To begin with, selection efficiency (efficiency that a signal event in the fiducial phase space is reconstructed in the detector) was compared, as Figure 6.

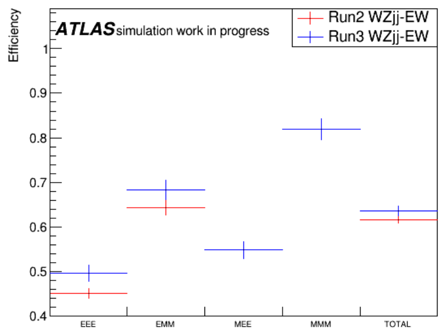

Figure 6: Comparison between Run-2 and Run-3 of selection efficiency (Reconstructed level/Fiducial phase space, generator level in WZjj-EW. It mainly depends on the detector efficiency).

The current selection efficiencies are mostly higher in Run-3 than in Run-2. In starting point for future optimization studies, it's good to use similar or identical lepton identification and isolation operating points for Run-2 and Run-3.

6.2 Comparison of kinematic variables

Kinematic variables important for the analysis are compared between Run-2 and Run-3 both in WZjj-EW signal and WZjj-QCD main background. To compare quantitatively, chi-square and p-value[12] were used. Chi-square χ^2 is defined as below:

$$\chi^2 = \sum_{x \in \{X\}} \frac{(y(x) - f(x))^2}{\sigma^2(x)} \tag{2}$$

(x : bin, X : bins, y : target histogram, f : compared histogram, σ : variance of each bin)

Comparison plots of kinematic variables related to the tagging jets and number of jets are Figure 7.

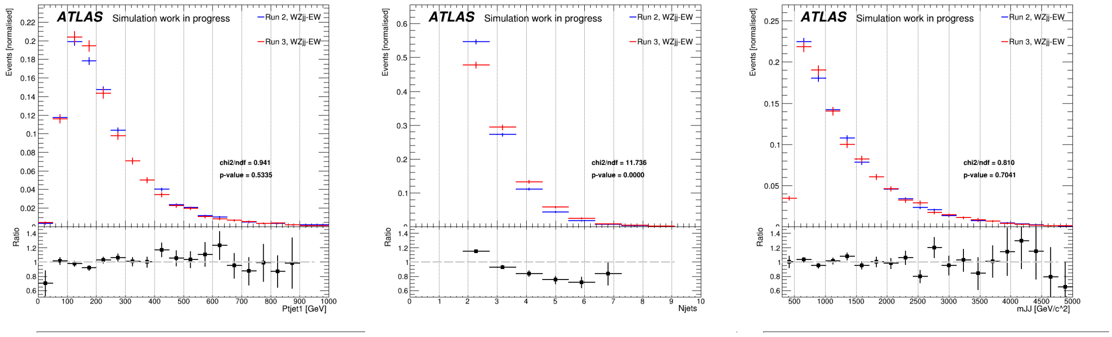

Figure 7: Comparison of pTjet1 (transverse momentum of the first jet), Njets (number of jets), mJJ (invariant mass of the two tagging jets) in WZjj-EW events.

Run-2 and Run-3 simulation have agreements in most variables like pTjet1 and mJJ, but not in variables related to jet multiplicity like Njets. Comparison plots of kinematic variables related to the third jet are Figure 8.

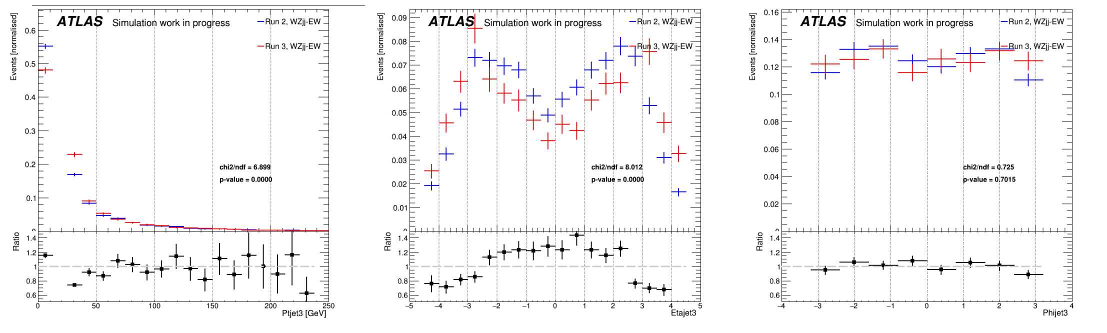

Figure 8: Comparison of pTjet3 (transverse momentum of no-tagged jet), Etajet3 (η of no-tagged jet), Phijet3 (ϕ of no-tagged jet) in WZjj-EW events.

The low transverse momentum region of the third jet have disagreement between Run-2 and Run-3. The difference of the shapes of the histograms between Run-2 and Run-3 have been observed in Etajet3, especially $|\eta| > 2.5$, but Phijet3 has good agreement. Etajet3 in WZjj-QCD events are also compared between Run-2 and Run-3 as Figure 9.

In WZjj-QCD events, the shape difference of Etajet3 can be easily seen. Run-3 events seem to have peaks around $|\eta| = 2.5$, which are not in Run-2 events.

6.2.1 Fiducial phase space

The disagreement we observe in Njets, pTjet3 and etajet3 are investigated. Those variables related to jet multiplicity generated in fiducial phase space (at generated level) are checked as Figure 10.

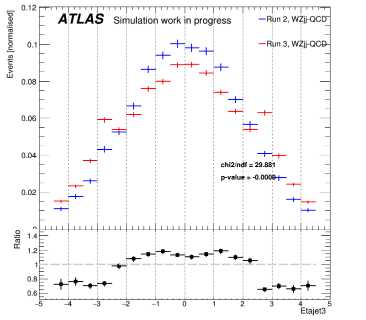

Figure 9: Comparison of Etajet3 in WZjj-QCD events.

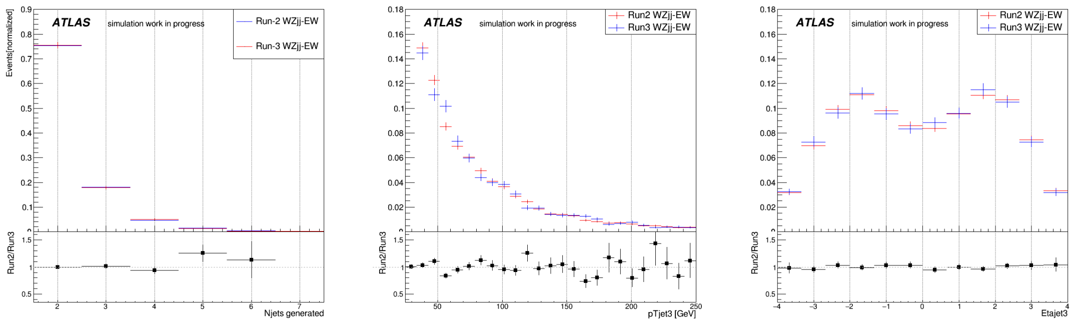

Figure 10: Comparison of Njets, pTjet3, Etajet3 between Run-2 and Run-3 at generated level in WZjj-EW events.

Better agreement is observed for variables related to jet multiplicity at generated level. Hence the problem of jets happens only at reconstructed level.

Investigating further, the number of reconstructed jets when the number of generated jets equals to 2 or 3 were checked.

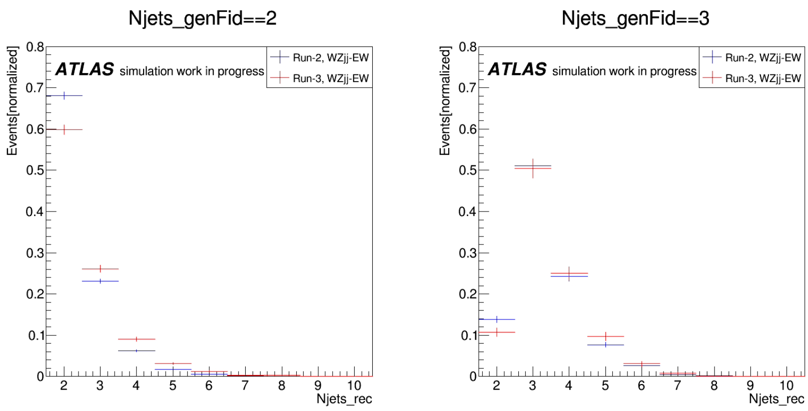

Figure 11: Njets at reconstructed level when Njets at generated level equals to 2, 3 in WZjj-EW events.

There are differences between Run-2 and Run-3 events. There seems to be some migrations from smaller Njets at generated level to bigger Njets at reconstructed level in Run-3 simulated events.

6.2.2 Reconstructed events with pT cut

The difference in the variables appears at reconstruction level seems to be related to the jet selection. Typically, excess of reconstructed jets, especially at low pT and in the forward direction is what one would observe when jets from pile-up are not properly rejected.

Then how the distribution changed when the transverse momentum of the third jet is bigger than 40 GeV were checked as Figure 12.

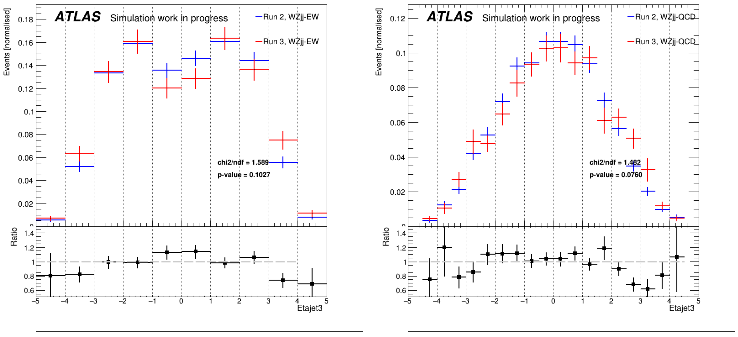

Figure 12: Comparison of Etajet3 between Run-2 and Run-3 in WZjj-EW events (left) and in WZjj-QCD events (right) with the cut of pTjet3$\geq$ 40 GeV.

Figure 12 shows that Etajet3 agree better after applying a cut on pTjet3$\geq$40 GeV. The plot of Etajet3 in WZjj-QCD also shows that the peaks around $|\eta| = 2.5$ disappear with this pT cut.

It was discovered that jet vertex tagger (identifying and rejecting jets whose origin does not come from the primary vertex) in forward region hasn't applied appropriately only in Run-3 data, hence jets in forward region ($|\eta| > 2.5$) with low pT are not only made by normal hard scatter, but also by pile up[12] in Run-3 simulated data. This has to be investigated further, however, currently, the forward jet vertex tagging selections are not available for Run-3 yet.

In conclusion, pile up can have impacts on many kinematic variables especially related to jet multiplicity. We need to be careful of handling of jets reconstruction.

6.3 Comparison of polarization variables

Polarization variables are compared between Run-2 and Run-3. Definition of the polarization angle $\cos\theta_{\mathrm{W(Z)}}$ is as Figure 13[7].

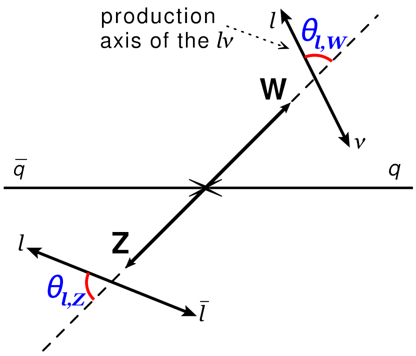

Figure 13: Definition of $\cos\theta_{\mathrm{W(Z)}}$.

We can determine the boson polarization fraction by measuring angles and kinematic distributions of the boson decay products.

Current distribution of polarization in simulated events at reconstruction levels as Figure 14.

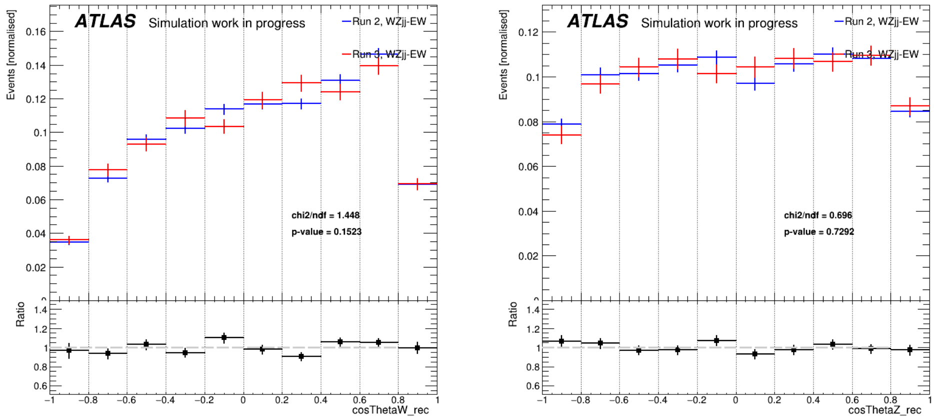

Figure 14: $\cos\theta_{\mathrm{W}}$ and $\cos\theta_{\mathrm{Z}}$ in WZjj-EW events.

There are small differences between Run-2 and Run-3 but they could be explained by:

- Slight changes in polarization fractions (due to the change of collision center-of-,ass energy, but not expected to be big as we have already seen)
- Different acceptances of the polarization fractions
- Different ratios of reconstructed W+Z and W-Z events
- pile-up jet issue (see 6.2.2)

Overall, they have good agreements between Run-2 and Run-3. Pile up doesn't seem to have a huge impact on the polarization variables.

7. Tagging Selection Optimization

Since the signal events are so rare, it is important to optimize the event and object selection to increase the signal to background ratio in the signal region so that the impact of the background uncertainties are reduced.

7.1 b-tagging optimization

Generally, signal events are not expected to contain jets from b-hadrons, but some background events like ttbar, tZ and ttV events are expected. In the signal region selection, a veto on b-tagged jets is applied. Optimizing the b-tagging efficiency operating point used for the veto can increase the signal-to-background ratio. In ATLAS, jets from b-hadrons are identified using a b-tagging algorithm. The latest for Run-3 data is the GN2 algorithm[13], where version GN2v00 is available in the current datasets. Different working points identify b-jets with an efficiency of $89\%, 85\%, 82\%, 77\%, 76\%, 70\%, 68\%, 60\%$ (Legacy and Alias operating points). GN2 tagger has a larger performance than the past tagger DL1r[14] used in Run-2.

We need to select the best trade-off between signal efficiency and background rejection. We use $\frac{S}{\sqrt{S+B}}$ (S:signal, B:background) as estimator. The results of each efficiency is as Figure 15.

According to the plot, 77% b-tagging efficiency is the best trade off. GN2v00 will switch to GN2v01 as soon as available in the skimmed datasets. It's slightly more performant in terms of mis-tagging rates. While the decrease in signal efficiency is not too large with respect to the losest operating point (60 %), it manages to well reject background such that the cut-based significance ($\frac{S}{\sqrt{S+B}}$) is maximal for that b-tagging operating point.

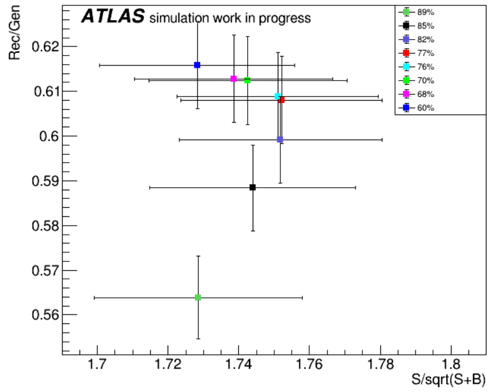

Figure 15: Ratio of signal efficiency to reconstruction efficiency in selected b-tagging efficiencies.

7.2 Quark-Gluon tagging optimization

To reject dominant background (WZjj-QCD) more strictly, we can optimize Quark-Gluon tagging efficiency. The two tagging jets in signal events are expected to be quark jets while this is not necessarily the case for background events, so optimization of Quark-Gluon tagger could lead to enrich the signal events. We used a preliminary version of the ATLAS quark-gluon tagger[15]. It is currently in active development in ATLAS. The operating points available to us are $90\%, 80\%, 70\%$.

Since the variables needed for the tagger are not yet available in the samples,, we applied it by using the efficiency maps. The efficiencies of quark-tagging we evaluated are $90\%, 80\%, 70\%, 95\%$. We only have the efficiency map of $90\%, 80\%, 70\%$. In 95% data point, the gluon tagging efficiency map is the same as 90%'s map so that it's a "toy" data point. We applied the QG-tagging by following method:

1. Check whether selected VBS tagging jets are gluon (PDGID=21) or a quark ($0 \leq$PDGID≤ 5)
2. Read efficiency from map (= probability p ($0 \leq p \leq 1$) that jet passes quark-gluon tagger selection)
3. Throw random number between 0 and 1, if rand $<$ p, jet passes quark gluon tagging selection
4. Both tagging jets need to pass quarks-gluon tagging selection

The result is as Figure 16.

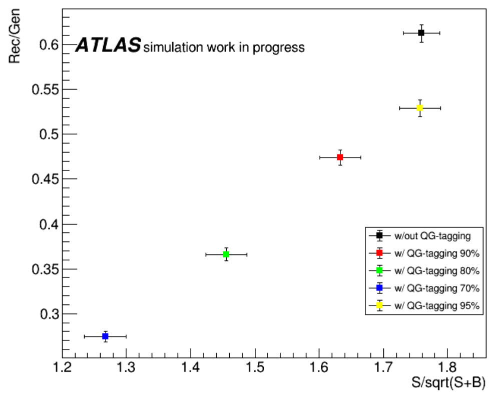

Figure 16: Ratio of signal efficiency to reconstruction efficiency in selected QG-tagging efficiencies.

Currently we lose too much events with the Quark-Gluon tagger. Our analysis does not benefit from it. Since the toy data point of 95 % quark efficiency gives currently the best result, it can be concluded that the analysis potentially profits from a more performant quark-gluon tagger with larger quark efficiency and better gluon rejection.

8. Conclusions

For accurate analysis of WZjj-EW events using ATLAS data, it is important to validate the simulated events. First, the ATLAS Run-3 data and simulated events are compared in each control region. The current modeling of ATLAS Run-3 simulated data is mostly good in the control regions, except in ZZ-CR whose normalization has to be investigated further. ATLAS Run-2 and Run-3 simulated events of WZjj-EW and WZjj-QCD are also compared for validation. Most variables have good agreement between Run-2 and Run-3, but not in variables related to jet multiplicity, especially the third jets in the forward region with low pT. It seems to be caused by pile up. We need to be careful of pile up to avoid its influence on some kinematic variables. In addition, selection efficiencies of Run-2 and Run-3 are found to be similar but a little bit higher in general for Run-3 in first look in simulation. We can use equivalent lepton identification or isolation selections in the first point of optimization.

Since the signal is a rare event, finding discriminating variables leads to more accurate analysis. Some kinematic variables are compared between the signal WZjj-EW and the dominant background WZjj-QCD. Some variables such that m_{JJ} and $Deta_{\mathrm{JJ}}$ are found to have decent discriminating power. We can use deep neural network by using the discriminating variables in the future.

It is also important to optimize tagging efficiencies to enrich the signal so that the uncertainty of the signal is reduced. 8 working points with different efficiency of b-tagging algorithm, GN2v00 tagger, are evaluated. It looks like we can tighten the veto on b-tagged jets slightly and go from 70% to 77% b-tagging efficiency with the new taggers. We also started to apply the new Quark-Gluon tagger, but currently we don't have benefit from it. Further investigation will be followed.

References

[1] ATLAS Collaboration. 'The ATLAS Experiment at the CERN Large Hadron Collider'. In: *Journal of Instrumentation* 3.08 (Aug. 2008), S08003. DOI: 10.1088/1748-0221/3/08/S08003. URL: https://dx.doi.org/10.1088/1748-0221/3/08/S08003.

[2] ATLAS Collaboration. 'Observation of a new particle in the search for the Standard Model Higgs boson with the ATLAS detector at the LHC'. In: *Physics Letters B* 716.1 (Sept. 2012), pp. 1–29. ISSN: 0370-2693. DOI: 10.1016/j.physletb.2012.08.020. URL: http://dx.doi.org/10.1016/j.physletb.2012.08.020.

[3] CMS Collaboration. 'Observation of a new boson at a mass of 125 GeV with the CMS experiment at the LHC'. In: *Physics Letters B* 716.1 (2012), pp. 30–61. ISSN: 0370-2693. DOI: https://doi.org/10.1016/j.physletb.2012.08.021. URL: https://www.sciencedirect.com/science/article/pii/S0370269312008581.

[4] CMS collaboration. 'Observation of Electroweak Production of Same-Sign W Boson Pairs in the Two Jet and Two Same-Sign Lepton Final State in Proton-Proton Collisions at $\sqrt{s} = 13$ TeV'. In: *Phys. Rev. Lett.* 120 (8 Feb. 2018), p. 081801. DOI: 10.1103/PhysRevLett.120.081801. URL: https://link.aps.org/doi/10.1103/PhysRevLett.120.081801.

[5] ATLAS collaboration. 'Observation of electroweak W±Z boson pair production in association with two jets in pp collisions at s=13 TeV with the ATLAS detector'. In: *Physics Letters B* 793 (2019), pp. 469–492. ISSN: 0370-2693. DOI: https://doi.org/10.1016/j.physletb.2019.05.012. URL: https://www.sciencedirect.com/science/article/pii/S0370269319303211.

[6] CMS collaboration. 'Measurements of production cross sections of WZ and same-sign WW boson pairs in association with two jets in proton-proton collisions at s=13TeV'. In: *Physics Letters B* 809 (2020), p. 135710. ISSN: 0370-2693. DOI: https://doi.org/10.1016/j.physletb.2020.135710. URL: https://www.sciencedirect.com/science/article/pii/S037026932030513X.

[7] ATLAS collaboration. 'Measurement of $W^{\pm}Z$ production cross sections and gauge boson polarisation in pp collisions at $\sqrt{s}$ = 13TeV with the ATLAS detector'. In: *The European Physical Journal C* 79 (2019), p. 535. ISSN: 1434-6052. DOI: 10.1140/epjc/s10052-019-7027-6. URL: https://doi.org/10.1140/epjc/s10052-019-7027-6.

[8] ATLAS collaboration. 'Observation of gauge boson joint-polarisation states in W±Z production from pp collisions at s=13 TeV with the ATLAS detector'. In: *Physics Letters B* 843 (2023), p. 137895. ISSN: 0370-2693. DOI: https://doi.org/10.1016/j.physletb.2023.137895. URL: https://www.sciencedirect.com/science/article/pii/S0370269323002290.

[9] ATLAS collaboration. 'Measurements of electroweak $W^{\pm}Z$ boson pair production in association with two jets in pp collisions at $\sqrt{s}$=13 TeV with the ATLAS detector'. In: *Journal of High Energy Physics* 2024 (2024), p. 192. ISSN: 1029-8479. DOI: 10.1007/JHEP06(2024)192. URL: https://doi.org/10.1007/JHEP06(2024)192.

[10] A. Hoecker et al. *TMVA - Toolkit for Multivariate Data Analysis*. 2009. arXiv: physics/0703039 [physics.data-an]. URL: https://arxiv.org/abs/physics/0703039.

[11] Enrico Bothmann et al. 'Event generation with Sherpa 2.2'. In: *SciPost Physics* 7.3 (Sept. 2019). ISSN: 2542-4653. DOI: 10.21468/scipostphys.7.3.034. URL: http://dx.doi.org/10.21468/SciPostPhys.7.3.034.

[12] Andy Buckley, Christopher White & Martin White. *Practical Collider Physics*. 2053-2563. IOP Publishing, 2021. ISBN: 978-0-7503-2444-1. DOI: 10.1088/978-0-7503-2444-1. URL: https://dx.doi.org/10.1088/978-0-7503-2444-1.

[13] ATLAS Collaboration. *Graph Neural Network Jet Flavour Tagging with the ATLAS Detector*. Tech. rep. All figures including auxiliary figures are available at https://atlas.web.cern.ch/Atlas/GROUPS/PHYSICS/PU PHYS-PUB-2022-027. Geneva: CERN, 2022. URL: https://cds.cern.ch/record/2811135.

[14] ATLAS collaboration. 'ATLAS flavour-tagging algorithms for the LHC Run 2 pp collision dataset'. In: *The European Physical Journal C* 83 (2023), p. 681. ISSN: 1434-6052. DOI: 10.1140/epjc/s10052-023-11699-1. URL: https://doi.org/10.1140/epjc/s10052-023-11699-1.

[15] ATLAS collaboration. *Constituent-Based Quark Gluon Tagging using Transformers with the ATLAS detector*. Tech. rep. All figures including auxiliary figures are available at https://atlas.web.cern.ch/Atlas/GROU PHYS-PUB-2023-032. Geneva: CERN, 2023. URL: https://cds.cern.ch/record/2878932.

Appendix

A. Searching for discriminating variables

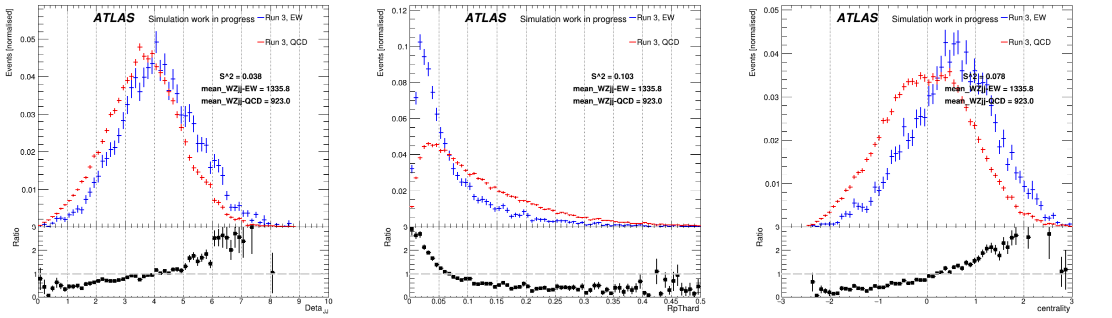

Figure A1: Comparison of WZjj-EW and WZjj-QCD using $\Delta\eta$ of the two selected tagging jets (left), RpThard (transverse component of the vector sum of W,Z and tagging jets momenta divided by their scalar pT sum)(center), and centrality (centrality of the WZ system)(right).

B. Comparison between Run-2 and Run-3

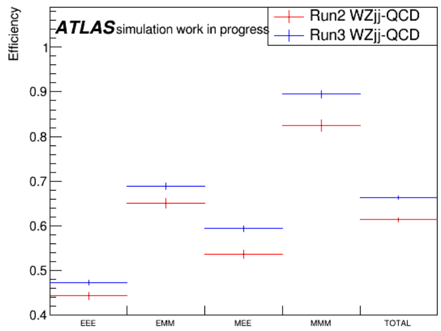

Figure B1: Comparison between Run-2 and Run-3 of selection efficiency (Reconstructed level/Fiducial phase space, generator level) in WZjj-QCD.

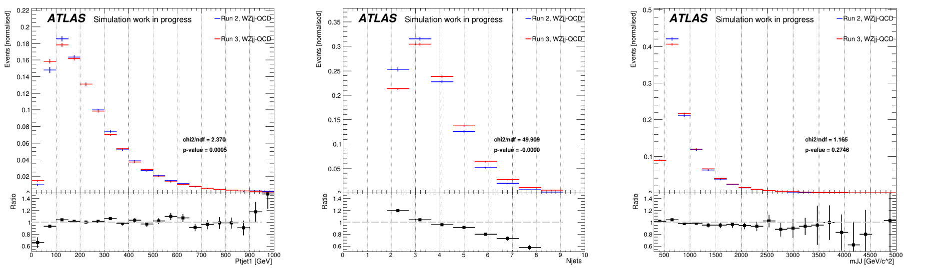

Figure B2: Comparison of pTjet1 (transverse momentum of the first jet), Njets (number of jets), mJJ (invariant mass of 2 jets) in WZjj-QCD events.

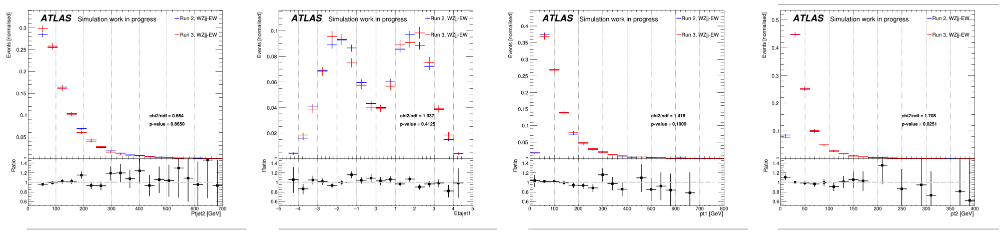

Figure B3: Comparison between Run-2 and Run-3 in WZjj-EW data. In the first row from the left side, Ptjet2(transverse momentum of Jet2), Etajet1(η of Jet1), Pt1(transverse momentum of the first lepton from the Z boson decay), Pt2(transverse momentum of the secomd lepton from the Z boson decay).

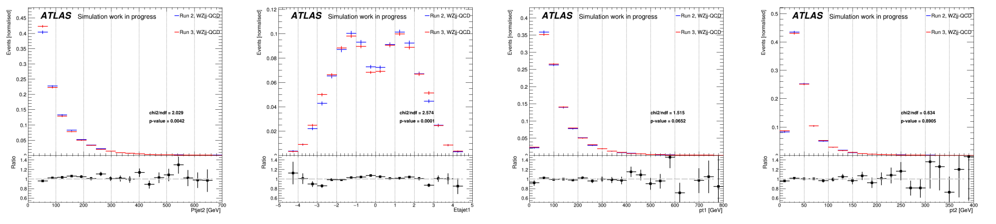

Figure B4: Comparison between Run-2 and Run-3 in WZjj-QCD data. In the first row from the left side, Ptjet2(transverse momentum of Jet2), Etajet1(η of Jet1), Pt1(transverse momentum of the first lepton from the Z boson decay), Pt2(transverse momentum of the secomd lepton from the Z boson decay).

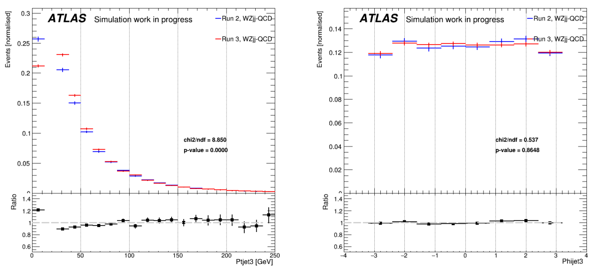

Figure B5: Comparison of pTjet3 (transverse momentum of no-tagged jet) and Phijet3 (ϕ of no-tagged jet) in WZjj-QCD events.

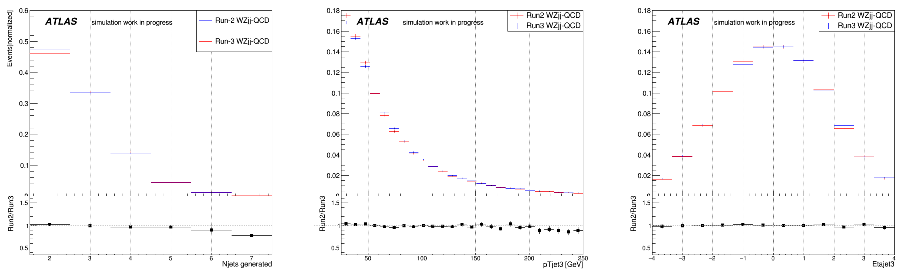

Figure B6: Comparison of Njets, pTjet3, Etajet3 between Run-2 and Run-3 at generated level in WZjj-QCD events.

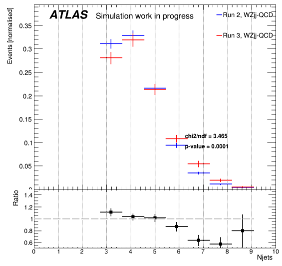

Figure B7: Comparison of Njets between Run-2 and Run-3 in WZjj-QCD events with the cut of pTjet3≥ 40 GeV.

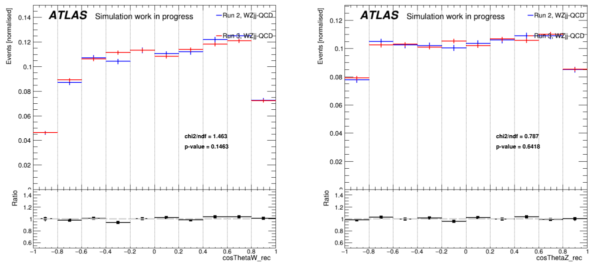

Figure B8: $\cos\theta_{\mathrm{W}}$ and $\cos\Theta_{\mathrm{Z}}$ in WZjj-QCD events.

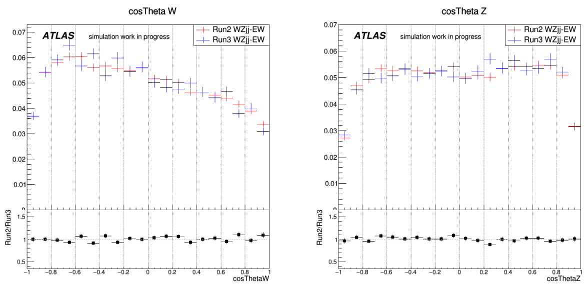

Figure B9: $\cos\theta_{\mathrm{W}}$ and $\cos\Theta_{\mathrm{Z}}$ at generate level in WZjj-EW events.

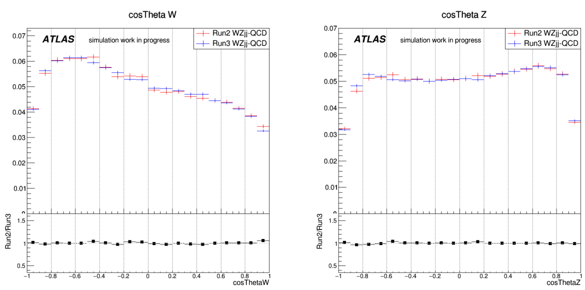

Figure B10: $\cos\theta_{\mathrm{W}}$ and $\cos\Theta_{\mathrm{Z}}$ at generate level in WZjj-QCD events.